2020-01-2034

Computational Study of a Multiple Fuel Injector Concept under High-Load and High-EGR Conditions

Rafig Babayev, Gustav Nyrenstedt, and Bengt Johansson
Clean Combustion Research Center (CCRC), King Abdullah University of Science and Technology (KAUST)

Abstract

A new concept utilizing multiple fuel injectors was proven effective at reducing heat transfer losses by directing spray plumes further away from the combustion chamber walls. In this concept, two injectors are mounted close to the rim of the piston bowl and point in opposite directions to generate swirling in-cylinder bulk motion. Moreover, a new flat-bowl piston design was also proposed in combination with the multiple fuel injectors for even larger improvements in thermal efficiency. However, all tests were performed at low-to-medium load conditions with no significant EGR. Modern engine concepts, such as the double compression-expansion engine (DCEE), have demonstrated higher thermal efficiency when operated at high-load conditions with a large amount of EGR for NOx control. Thus, this study aims to assess the effectiveness of the multiple-fuel-injector system under such conditions. In this study, a number of 3-D CFD simulations are performed using the RANS technique in CONVERGE. The computational domain is based on the modified Volvo D13 engine geometry that is used as a combustor unit of the DCEE. The results of this study show that the injection strategies used previously with the multiple-fuel-injector concept perform poorly at high-load conditions due to inadequate mixing. Moreover, the flat-bowl piston design proposed previously does not seem to improve heat transfer losses at these conditions. Thus, several alternative piston bowl designs are investigated, some of which are shown to reduce heat losses and improve mixing. Finally, a number of perspective strategies are recommended to be implemented with the multiple-fuel-injector concept for efficiency maximization.

Introduction

Transport sector was responsible for about 27% of greenhouse gas (GHG) emissions from the EU in 2017 (including aviation and shipping) [1]. 72% of these emissions were from road transport, which is dominated by vehicles with internal combustion engines. Alternative transport modes are not expected to significantly reduce the life-cycle GHG emissions from the transport sector [2]. Heavy-duty (HD) diesel vehicles are responsible for about a quarter of CO_2 emissions from the transportation sector in the EU [3]. Owing to an anticipated 45% increase in demand for HD vehicles by 2040 [4] the CO_2 emissions from HD vehicles is only expected to increase in the near future. As a response to this pressing issue, in 2019 the European Commission has set the first EU-wide CO_2 emission standards for HD vehicles [5]. The targets of the new regulations are a 15% reduction in the fleet-wide average CO_2 emissions by 2025, and a 30% reduction by 2030, compared to the EU average in the reference period between July 1st 2019 and June 30th 2020.

Incremental improvements in engine efficiency might not be sufficient to meet the ever more strict regulatory targets mentioned above. Thus, a lot of research efforts nowadays are focused on designing new engine concepts fundamentally superior to conventional engines in terms of efficiency. Split-cycle engine configurations have been proven to be advantageous owing to the additional degrees of freedom that they offer for optimization [6-10]. One of the most recent and successful designs that may help automakers to meet the new targets is the double compression-expansion engine (DCEE), also known as the 8-stroke engine [11]. The layout of this engine concept is illustrated in Figure 1. This engine consists of three types of cylinders, two of which operate at relatively low pressures, while the third one operates at extremely high pressures. First, fresh air is compressed in the compressor unit, after which the air is transferred through a low-pressure (LP) tank into the combustor unit. The combustor unit is essentially a combustion cylinder of a conventional CI engine with the only exception of a lower compression ratio. In the combustor, the air is compressed again up to the pressures close to 300 bar, after which fuel injection and combustion occur. The combustor unit also accommodates the first stage of the expansion process. The size of the combustor unit is limited as much as possible to reduce heat transfer and mechanical losses. After the first stage of expansion in the combustor is over, the exhaust gases are further transferred through the high-pressure (HP) tank into the dedicated expander unit. There, the second stage of expansion is performed, in the end of which the gases are at near-atmospheric pressures. The expander cylinder has a notably large displacement and expansion ratio which enables a more efficient work extraction from a large amount of exhaust gas at relatively low pressures, while limiting the friction loss. After the final expansion is over, the gases are discharged into the atmosphere.

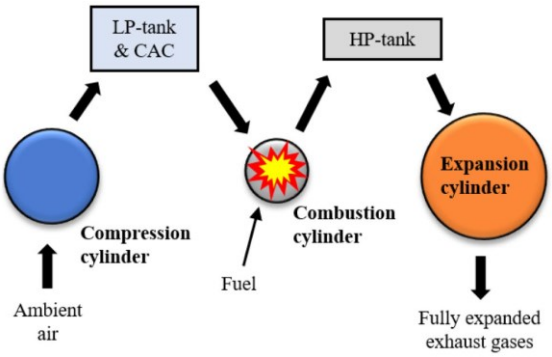

Figure 1. The DCEE concept layout [12].

Numerous studies have shown that the DCEE is capable of achieving brake thermal efficiency of 56% at higher load conditions (56 bar FuelMEP of the combustor unit). More recent developments have hinted even higher numbers, close to 60%. This is significantly higher than the thermal efficiency of even the best modern conventional powertrains, which makes the DCEE a highly attractive option for automakers in their pursuit of lower fleet-wide average CO_2 emissions.

One of the main advantages of the DCEE is its ability to use the exhaust gases of the combustor unit to generate extra useful work. Hence, the exhaust "loss" of the combustor unit cannot be considered as a loss in a conventional sense. However, the combustor unit's heat transfer loss is unrecoverable, thus most attempts to further increase the DCEE thermal efficiency are focused on reducing heat transfer losses. One strategy that was previously proposed for a simultaneous reduction of the heat transfer losses and NOx emissions is the isobaric combustion concept [13-14]. It also showed gross indicated efficiency values comparable to the conventional diesel combustion (CDC) with only a marginal penalty on soot emissions. However, the isobaric combustion concept requires complex split main injection strategies with short shot-to-shot separations. This puts great burden on the conventional fuel injection systems. Moreover, late injections at higher loads struggle with keeping the pressure constant due to faster expansion and heat losses.

The aforementioned issues might be solved by installing more than one injector per cylinder. Multiple fuel injector concepts have been studied before both computationally and experimentally. Some concepts focus on alleviating the drawbacks of pilot injections (such as elevated soot emissions) by equipping the engine with an additional common-rail fuel injector per cylinder, thus spatially separating the pilot from the main injection [15, 16]. In 2016, Okamoto and Uchida introduced a split fuel injector concept capable of spatially separating main injections too, equipping the engine with two additional side injectors per cylinder (Figure 2) [17]. They showed experimentally that heat release rate profile can be more easily controlled with multiple injectors. Moreover, a simultaneous reduction in both NOx and soot emissions was achieved with this system, which was explained by lower combustion temperatures and local equivalence ratios.

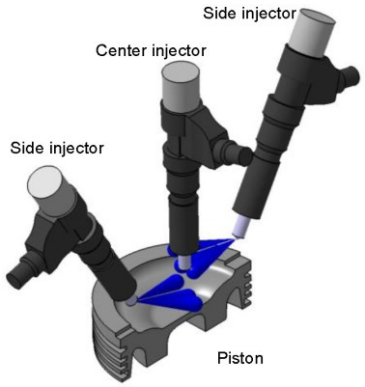

Figure 2. Layout of the DI system comprised of one central injector and two side injectors mounted at the bowl rim [17].

Nyrenstedt et al. [18] then studies this concept with the aid of RANS simulations and reported 13% lower heat transfer losses compared to a conventional single-injector system. The reduction was achieved when using two side injectors placed and the rim of the piston bowl. With this configuration, high temperature zones could be kept further away from the cylinder walls, thus reducing heat flux to them. In principle, the mechanism of heat loss and NOx emissions reduction is similar for the multiple-fuel-injector and isobaric combustion concepts.

The current paper extends the concept with two side fuel injectors to more relevant engine operating conditions. As briefly mentioned previously, the DCEE achieves its peak system efficiency at 56 bar FuelMEP for combustor unit, which approaches the maximum load capabilities of diesel engines. Also, this operating point requires 36.4% EGR to keep NOx emissions and heat losses under control [12]. These requirements challenge the side-injector concept, pushing it to the limits in terms of its mixture formation characteristics. This paper will assess potential of an engine equipped with side fuel injectors under high-load high-EGR conditions relevant for many modern engines, such as the DCEE.

Simulation Setup

All results in this study are obtained by performing three-dimensional RANS simulations using the CONVERGE CFD software [19]. The successive over-relaxation (SOR) method is used to solve the momentum, pressure, density, energy, and species equations. A variable time-step algorithm is implemented with the minimum time-step of 1E-8s and the maximum convection, diffusion, and Mach CFL limits of 1, 2, and 50, respectively. The Redlich-Kwong (RK) equation of state is used with the critical temperature of 133 K, and critical pressure of 3.77E+06 Pa. An AramcoMech reduced kinetic model for compression-ignition simulations of complex TPRF surrogate fuels [20] is solved using CVODES in the SAGE detailed chemistry solver. The kinetic model contains 61 species and 270 reactions. The injection process of the diesel fuel is modeled with a discrete phase model where a total of 420,000 drop parcels bearing physical properties of diesel fuel are introduced into the computational domain. Modeling of spray atomization and break-up is implemented using a hybrid Kelvin-Helmholtz (KH) and Rayleigh-Taylor (RT) model. The diesel fuel is evaporated using the Frossling model. After evaporation, the combustion chemistry of diesel fuel is approximated by n-heptane (n-C_7H_{16}). In this study, turbulence is modeled using RNG k-ε model with standard coefficients.

A structured cut-cell Cartesian grid is used with the base cell size of 2 mm. To reduce the computational cost while maintaining a high level of accuracy, adaptive mesh refinement (AMR) is used to reduce the

cell size down to 0.25 mm (scale 3) based on the velocity and temperature gradients. Additionally, grid embedding of scale 3 is applied in the region around the spray, whereas an embedding of scale 2 is laid over the cylinder boundaries. This choice of the boundary embedding is justified in the next subsection.

Heat Transfer Modeling

Due to computational cost considerations, the grid resolution near the walls in this study is not sufficient for accurate modeling of the viscous sublayer. Instead, the law-of-the-wall temperature boundary condition is implemented on all cylinder walls and heat transfer is modeled using the O'Rourke and Amsden model [21]. The wall heat transfer is calculated as per Equations 1-4.

$$k\frac{\partial T}{\partial x} = \frac{\mu_m c_p (T_g - T_w)}{Pr_m\, y} F \tag{1}$$

$$F = 1.0 \quad y^+ < 11.05 \tag{2}$$

$$F = \frac{\frac{y^+ Pr_m}{Pr_t}}{\frac{1}{\kappa}\ln y^+ + B + 11.05\left(\frac{Pr_m}{Pr_t} - 1\right)} \quad y^+ > 11.05 \tag{3}$$

$$y^+ = \frac{\rho u_\tau y}{\mu_m} \tag{4}$$

Where,

k – molecular conductivity,
μ_m – molecular viscosity,
T_g – gas temperature,
T_w – wall temperature,
y^+ – dimensionless wall distance,
y – absolute wall distance,
Pr_m – molecular Prandtl number,
Pr_t – turbulent Prandtl number,
u_τ – shear speed,
B – law-of-the-wall parameter equal to 5.5,
κ – Von Karman constant equal to 0.42.

As mentioned in the previous section, additional grid embedding of scale 2 (0.5 mm) was applied on all cylinder boundaries. This embedding scale value was chosen to keep the y^+ values within the range of 30 – 100 recommended for k-ε turbulence model. This enables the first cell center to be always located in the log-law region.

Experimental Setup and Operating Conditions

Experimental Setup

Experimental data used as a reference for setting up relevant boundary conditions in the simulation as well as for model validation was taken from the study by Lam et al. [12] on system brake efficiency of the DCEE concept. In their study, the combustor unit of the concept was investigated experimentally using a modified single-cylinder version of the Volvo D13 engine. Table 1 shows the specifications of the test engine. The specifications of the diesel fuel injector are given in Table 2.

Table 1. Test engine specifications.

Cylinder bore	0.131 m
Stroke	0.158 m
Con. Rod length	0.265 m
Crank offset	0 m
Compression ratio	11.5 : 1
Fuel system	Common-rail direct-injection

Table 2. Diesel fuel injector specifications.

Number of nozzle holes	7
Nozzle diameter	265 um
Spray cone angle	10 deg
Spray umbrella angle	145 deg
Discharge coefficient	0.9635

Operating Conditions

The combustor unit of the DCEE is almost identical in operation to a conventional four-stroke diesel engine. The main differences are the pressure during the inlet and exhaust strokes and the compression ratio, the former of which is significantly higher with the DCEE combustor unit, while the latter is considerably lower compared to modern diesel engines. This is to provide enough energy for the expander unit to operate efficiently. The operating conditions of the combustor unit at the load point corresponding to Case 9 reported by Lam et al. are given in Table 3. This operating point yielded the highest brake thermal efficiency for the whole DCEE system, hence was chosen as the most interesting case to investigate with the new multiple-injector concept.

Table 3. Operating conditions for the highest-efficiency case (Case 9) implemented experimentally [12].

Inlet pressure	5 bar
Inlet temperature	70 °C
Engine speed	1200 RPM
Injection pressure	2200 bar
Start of injection	-2.7 deg ATDC
Injection duration	1500 us or 10.8 CAD at 1200 RPM
Injected fuel mass	275.6 mg/cycle
EGR rate	36.4%
Air-fuel equivalence ratio (λ)	1.36
FuelMEP	55.8 bar
$IMEP_{gross}$	25.9 bar
$IMEP_{net}$	22.1 bar

CFD Model Validation

In this study, only the closed-volume part of the cycle was simulated. Thus, only the combustion cylinder was modeled (no intake and exhaust ports or valves). Some parameters required for setting up relevant conditions for closed-cycle 3-D CFD simulations are hard to obtain experimentally, hence, they were estimated using 1-D GT-Power simulations. This data is reported in Table 4.

Table 4. Operating conditions obtained using 1-D GT-Power simulations.

In-cylinder pressure at BDC	5.14 bar
In-cylinder temperature at BDC	127 deg C
Piston temperature	227 deg C
Liner temperature	207 deg C
Cylinder head temperature	227 deg C
In-cylinder composition at IVC (mass fractions)	
CO2	0.0945
H2O	0.0361
N2	0.7059
O2	0.1635

Even though the exact profile of the injection rate was not available to us, we made our best attempts at approximating the injection rate shape based on the previous experimental investigations on a similar injector [14]. The fuel injection rate employed in this study is shown in Figure 3.

To validate the CFD models employed in this study, a simulation was carried out on an engine geometry described in Tables 1 and 2, with boundary conditions reported in Tables 3 and 4. Then, the pressure trace and heat release data from the simulation were compared to those from the experiments. Figure 3 shows that the simulated pressure trace and heat release rate match almost perfectly with those obtained experimentally.

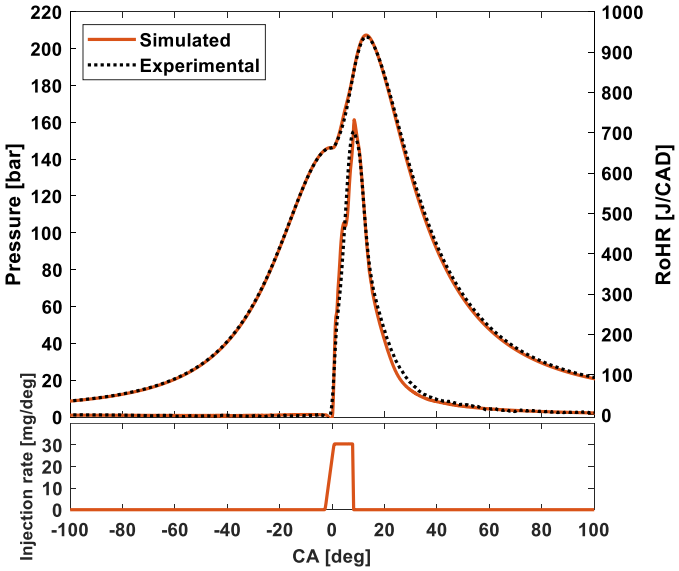

Figure 3. Comparison of the rate of heat release (RoHR), and pressure traces obtain experimentally and numerically.

Ignition delay, combustion phasing, gross IMEP, and equivalence ratio from the simulation were also compared to those from experiments, and the results are given in Table 5. An exceptionally good match is obtained with the aforementioned parameters too.

Table 5. Comparison of the ignition delay, combustion phasing (CA50), air-fuel equivalence ratio, and gross indicated mean effective pressure (IMEPgross) obtained experimentally and numerically.

	Experiments	**Simulations**
Ignition delay	2.2 deg	2.0 deg
CA 50	10.7 deg ATDC	10.4 deg ATDC
Air-fuel equivalence ratio (λ)	1.360	1.366
$IMEP_{gross}$	25.9 bar	25.9 bar

NOx Emissions

Emissions of nitrogen oxides (NOx) were measured by Lam et al. using an AVL AMAi60-system [12]. They report 0.41 g/kWh gross indicated specific NOx emissions for the 56 bar FuelMEP operating point, which was chosen as the experimental reference case in this study.

In the simulations performed for the current study, the Extended Zeldovich thermal NOx model [22] was employed. An equilibrium assumption was made on the O and OH radical concentrations. This assumption is justified by the fact that the kinetics of the thermal NOx formation are significantly slower than that of the hydrocarbon oxidation [23]. Thus, this assumption is typically valid for when combustion temperatures exceed 2200 K, which was the case most of the time for all simulations performed in this work.

The amount of NOx estimated by the simulations is 0.26 g/kWh. Taking into account that in experiments, 36.4% of exhaust gas was recirculated back into the inlet, the emissions analyzer also measured the NOx contained in the EGR in addition to the NOx generated by combustion. However, the inlet gas composition imposed in simulations did not contain any NOx, hence, the simulated exhaust gas contains NOx only from combustion (no recirculated NOx that is present in experiments), yielding lower values. These discrepancies between simulations and experiments are compensated for by adjusting the simulated NOx according to Equation 5.

$$S_{NOx-sim.+EGR} = S_{NOx-sim.} + S_{NOx-sim.} * EGR_{rate} \quad (5)$$

Where,

$S_{NOx-sim.}$ – simulated NOx emissions in g/kWh,
$S_{NOx-sim.+EGR}$ – simulated NOx emissions plus NOx from EGR in g/kWh,
EGR_{rate} – fraction of the exhaust gas recirculated back into the inlet as reported by Lam et al.

After compensating for EGR, the NOx emissions from simulations become *0.36 g/kWh*, which is sufficiently close to the experimentally measured value of *0.41 g/kWh*. Note that no tuning of the NOx model was required to achieve this match.

Results and Discussion

Three-dimensional data shown in this section was visualized using ParaView scientific visualization software [24]. In order to depict the flame plumes, contour plots of equivalence ratio of 0.8, 1.0, and 1.2 were generated and colored with temperature.

Multiple Fuel Injectors

In the experiments conducted by Lam et al. the number of holes in the central injector nozzle was seven. However, to enable a direct comparison between the conventional central injector and the double-side-injector configurations, the number of nozzle holes of the conventional injector in this study was reduced to six to yield an even number. This configuration was simulated at the same conditions as in the "CFD Model Validation" section. The only change that had to be made is the injection duration, which was increased to compensate for the reduced number of holes maintaining a constant discharge coefficient. As a result of this adjustment, the $IMEP_{gross}$ reduced from 25.90 bar to 25.66 bar. Henceforward, the central-injector case with

six nozzle holes will be considered as a reference for comparison to a conventional injector configuration.

Figure 4 illustrates both the double-side-injector and the conventional central-injector configurations in the same cylinder, where the white cones represent the direction and cone angle of the sprays.

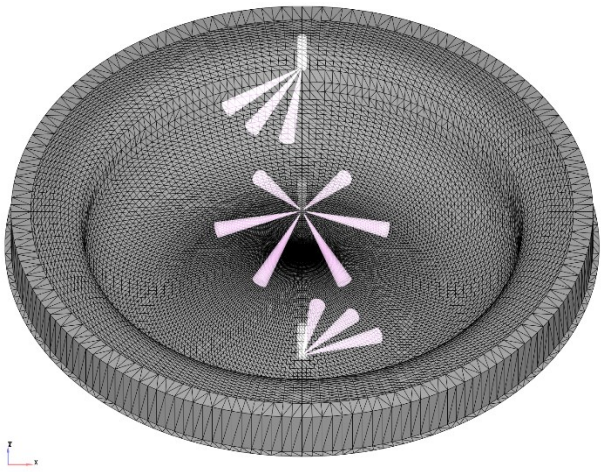

Figure 4. Conventional central- and double-side-injector configurations shown in the same cylinder, along with the piston crown at TDC.

Double-Side-Injector Configuration

In this section the double-side-injector configuration is compared to the single-central-injector configuration. The spray and flame plumes from the former one are presented in Figure 5.

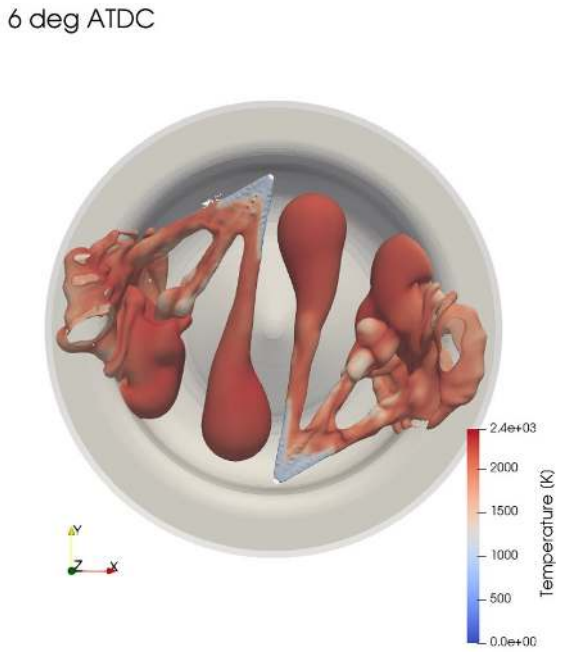

Figure 5. Flame plumes created by two side injectors at 6 CAD ATDC.

Figure 6 illustrates the injection rate, heat release, and pressure trace for the single-central- and the double-side-injector configurations. From this figure it can be seen that the heat release of the case with two side injectors is less favorable than that of the single-injector case. The former reaches a plateau after around 5 CAD ATDC, which prevents it from reaching values as high as those achieved by the latter.

The heat release rate from the side injectors also drops much faster once the fuel injection is stopped; however, the overall burning duration is significantly longer. As can be seen from Table 6, the double-side-injector case has similar CA50, but much later CA90. As a result, the tail of the heat release contributes to over 3 %p reduction in indicated efficiency.

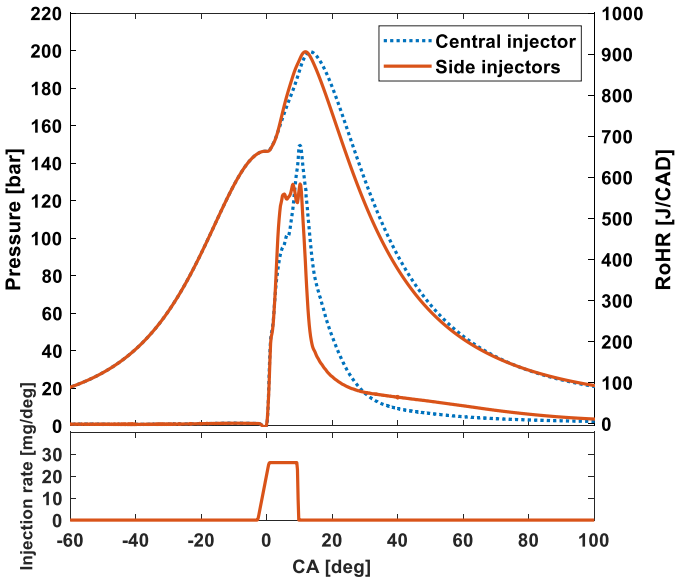

Figure 6. Injection rate, rate of heat release (RoHR), and pressure traces for the reference central injector and the double-side-injector configurations.

Table 6. Gross indicated mean effective pressure ($IMEP_{gross}$), gross indicated efficiency (GIE), crank angle of 50% heat release (CA50), and crank angle of 90% heat release (CA90) for the reference central injector and the double-side-injector configurations.

	1 central injector	2 side injectors
$IMEP_{gross}$ [bar]	25.66	23.80
GIE [%]	44.2	41.0
CA50 [deg ATDC]	11.4	11.2
CA90 [deg ATDC]	25.2	52.2

The heat that is not released in the early stage of combustion is released later, in the tail of the RoHR. A number of reasons might be contributing to such behavior. One of them might be wall wetting from two sprays that are the closest to the walls. In order to find out whether this is the case, the injector configuration and the liquid spray penetration are plotted and illustrated in Figures 7 and 8, respectively.

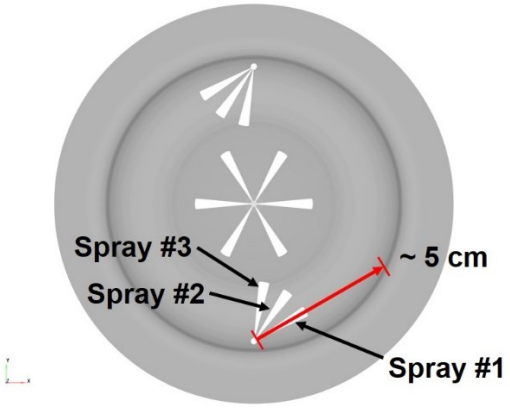

Figure 7. Injector configurations depicted relative to the piston.

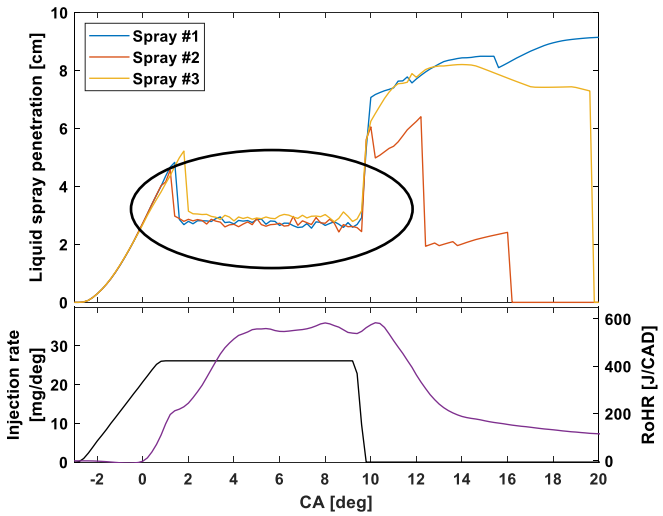

Figure 8. Injection rate, rate of heat release, and liquid spray penetration from each of the sprays depicted in Figure 7.

As can be seen from Figures 7 and 8, the liquid spray penetration during the injection process is only 3 cm, which is much shorter than the distance between the nozzle and the piston bowl (~5 cm). It is also approximately equal for all three sprays. This suggests that none of the sprays reach the piston bowl. Furthermore, later in the paper, it will be shown that reducing the angle between the nozzle-hole axes, thus directing the sprays further away from the walls may still lead to similar results in terms of heat release. Thus, it is concluded, that the adverse heat release and reduction in IMEP is not because of the wall wetting.

There are two important observations that can be made from Figure 5. First, the sprays that are the closest to the piston surface (Spray #1 and its counterpart from the other injector) are directed toward the walls. This results in the plume/wall impingement and the consequent redirection of the two side plumes toward the neighboring ones. As a results, a significant plume-to-plume interaction takes place. The second observation is a substantially smaller volume occupied by the flames with the double-side-injector configuration. Both phenomena are illustrated in Figure 9.

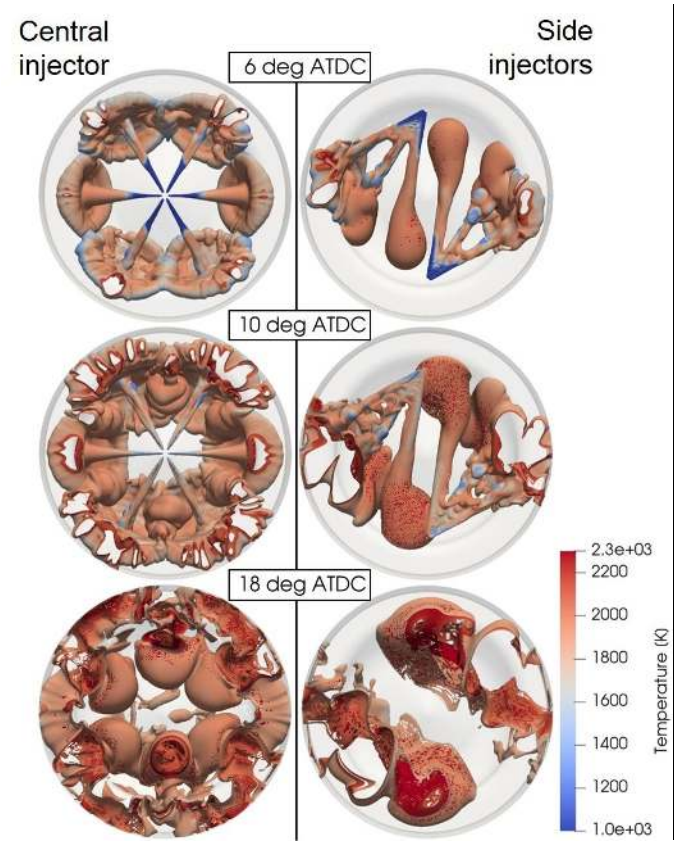

Figure 9. Comparison of the flame plumes generated by the conventional central injector and double-side-injector configurations.

As can be observed from Figure 9, the resultant reaction zone size is much smaller with the double-side-injector configuration compared to the single-central one. This is partly due to the piston bowl shape un-optimized for the non-axisymmetric injector configuration, which results in significantly inferior mixing characteristics, hence limited heat release. Another factor contributing to slow heat release is the plume-to-plume interaction that was discussed in the previous paragraph. Both phenomena lead to higher local equivalence ratios and overall declined fresh air utilization.

Combustion efficiency reduced by about 1%. However, the long tail in HR leads to an inferior thermodynamic cycle and a reduction in IMEP of about 7%. This translates into a reduction of 3.2 %p in gross indicated efficiency. The relative distribution of fuel energy is calculated and presented in Figure 10.

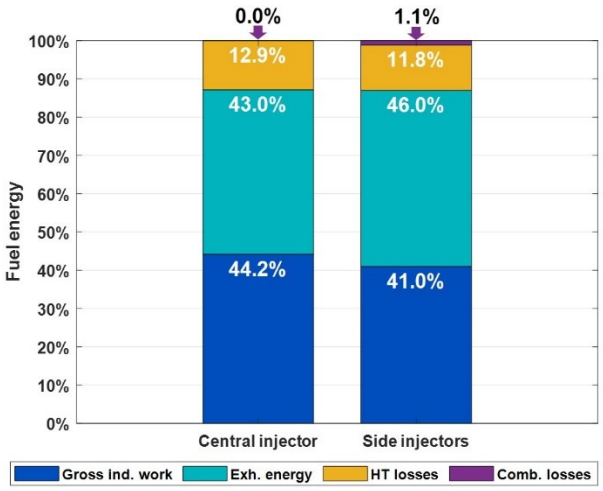

Figure 10. Fuel energy distribution between work on the piston, exhaust enthalpy, heat transfer losses, and combustion losses for the reference central injector and the double-side-injector configurations.

It can be observed from Figure 10 that, even though the gross indicated work reduced with the side-injector configuration, the heat transfer losses underwent a significant reduction as well. It has previously been reported by Nyrenstedt et al. that heat transfer losses can be drastically reduced with a two-injector system [25]. In order to understand the reason behind the reduced heat transfer losses, the heat flux to the piston, head, and liner surfaces was calculated using the methods described in the "Computational Methodology" section. The results of the calculations are presented in Figure 11.

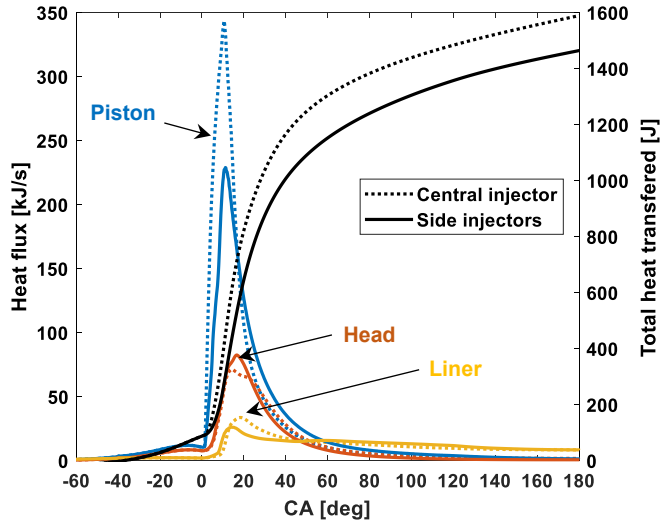

Figure 11. Heat flux to the piston, head, and liner surfaces, and the total amount of heat transferred to all cylinder walls combined for the reference central injector and the double-side-injector configurations.

Figure 11 shows that the total heat transfer loss is reduced by 8% with the side-injector configuration compared to the central. This is about 1% of the fuel energy. Most of the reduction comes from the piston boundary. Comparing the central- and side-injector cases from Figure 9, one can immediately see that in the former case, all six spray plumes are directed perpendicularly to the piston bowl resulting in an extensive plume-wall impingement. This enhances the mixing of the fuel with fresh air, promoting faster combustion. However, this also causes much larger heat flux to the piston surface, as can be seen in Figure 11. The overall size of the high-temperature zone is much smaller with the side-injector configuration, where flames are mainly concentrated in two relatively small "clouds" mostly inside the piston bowl, which positively affects heat losses. Also, the in-cylinder temperature is significantly lower with the side-injector system in the earlier part of the cycle, as can be seen from Figure 12. This also contributes to the reduction in heat losses, since the convection heat transfer coefficient is the highest early in the expansion stroke.

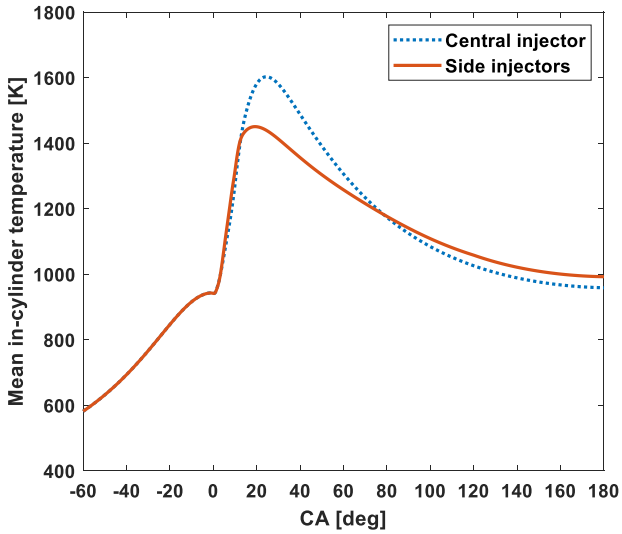

Figure 12. Mean in-cylinder temperature for the reference central injector and the double-side-injector configurations.

These results confirm the finding of the work by Nyrenstedt et al. at medium loads, and suggest that, if done correctly, the side-injector concept has a potential to increase engine efficiency by reducing heat transfer losses even at higher engine load conditions.

Various Piston Bowl Designs

Flat Piston Bowl Geometries

Flat Bowl V1

The idea behind using flat piston bowl is that the omega-shaped piston bowl normally used in modern diesel engines is not necessary with the side-injector configuration since the spray plumes are not directed toward the piston bowl in the same way as they are with the central injector. Then, having flat bowl, in theory, should enable lower heat transfer losses owing to reduced surface area [25]. In this subsection, the flat piston bowl geometry (Figure 13) is compared to the standard omega-shaped bowl with two side injectors.

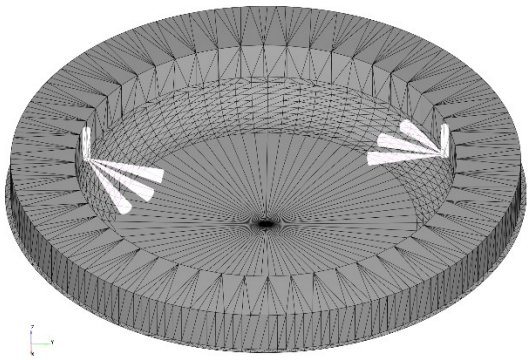

Figure 13. Flat piston bowl proposed by Nyrenstedt et al. [25] (Flat bowl V1).

The flat piston bowl does not seem to significantly affect the heat release and pressure traces, as they are practically identical to those with the standard piston bowl. The IMEP is reduced by a mere 0.1 bar. However, looking at the heat flux to the cylinder walls, notable changes can be observed. As can be seen in Figure 14, heat flux to the piston is reduced, while heat flux to the head is increased. Overall heat loss from the in-cylinder gas is relatively unchanged.

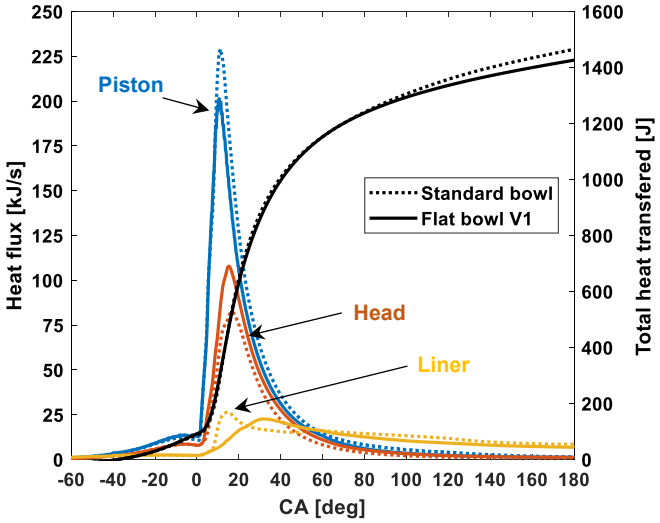

Figure 14. Heat flux to the piston, head, and liner surfaces, and the total amount of heat transferred to all cylinder walls combined for the standard omega-shaped piston bowl and the novel flat piston bowl (Flat bowl V1) with side injectors.

In an attempt to understand the reason for the reduction of heat flux to the piston and the increase of heat flux to the head, we made a 3-D plot of the flame plumes mid-injection and compared them for the Standard bowl and the Flat bowl V1 cases. The results are illustrated in Figure 15.

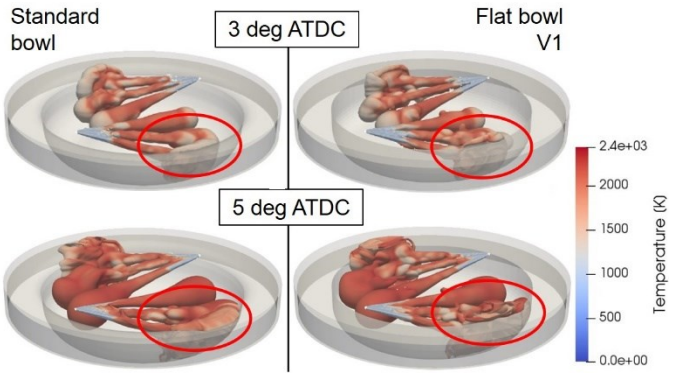

Figure 15. Comparison of the flame plumes generated by the side injectors with the standard omega-shaped piston bowl and the novel flat piston bowl (Flat bowl V1).

As can be seen from Figure 15, the bowl rim (the sharp edge between the piston bowl and the top land) of the Flat bowl V1 causes the flame plume to bounce off the piston bowl and hit the cylinder head. The flame then stays attached to the head leading to the increased heat losses. This is not the case with the standard piston which has a more gradual transition from the bowl to the top land area. This suggests that the reason for reductions in heat transfer losses to the piston in the Flat bowl V1 case might actually be the sharp bowl rim.

Flat Bowl V2

In order to confirm the aforementioned statement and, possibly, reduce the heat loss to the cylinder head, we propose the Flat bowl V2 geometry, which is illustrated in Figure 16. In the Flat bowl V2 variant the sharp bowl rim is removed. Instead, a more gradual transition is implemented, similar to the bowl rim found in the standard omega-shaped pistons. This change should help direct the plumes away from the head, thus reducing the heat loss.

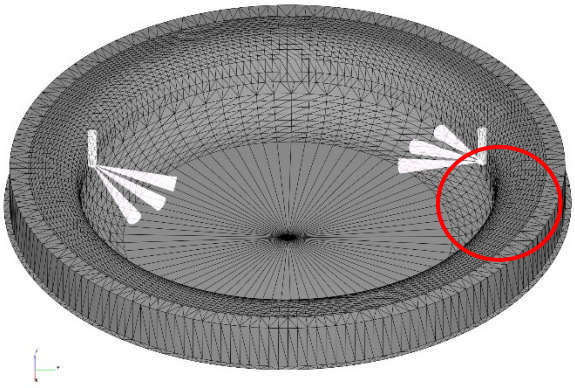

Figure 16. The new proposed flat piston bowl (Flat bowl V2) to be used with the double-side-injector concept.

Figure 17 shows that the heat flux to the piston for the Flat bowl V2 case increased compared to the Flat bowl V1, and reached almost the same values as for the standard bowl design. Furthermore, the total heat transfer losses to all boundaries look remarkably similar for the Standard bowl and the Flat bowl V2. Only a slight reduction of about 1% is observed with the Flat bowl V2. The fact that the heat flux is nearly equal for the Standard bowl and the Flat bowl V2 confirms that the surface area of the piston bowl does not significantly affect the heat transfer losses. Instead, the flow pattern generated by the shape of the bowl and, more specifically, the bowl rim plays a larger role in determining the losses.

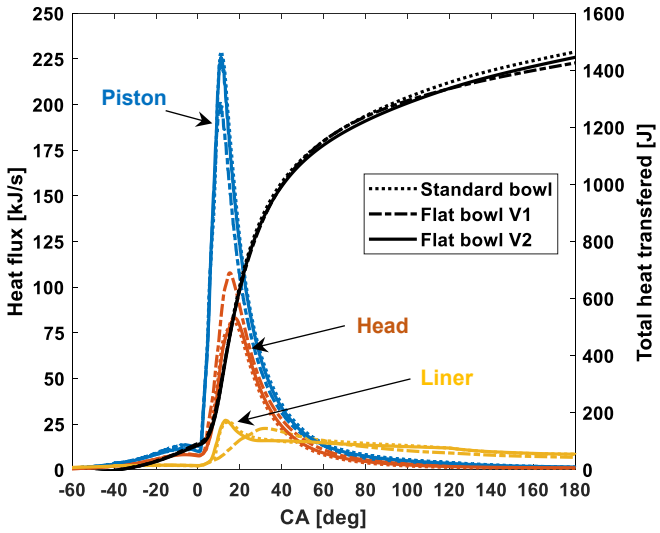

Figure 17. Heat flux to the piston, head, and liner surfaces, and the total amount of heat transferred to all cylinder walls combined for the standard omega-shaped piston bowl, Flat bowl V1, and Flat bowl V2.

These results are different to the previous findings of Nyrenstedt et al. [25]. In their study, heat losses were reduced because of the smaller piston area. However, fueling in their cases was much lower (150 mg

vs 275.6 mg in this study) and, consequently, either the injection duration was shorter or the injection pressure was lower. Taking that into account, it is reasonable to assume that in their case, the flame plumes did not attach to the head as much as they did for our cases, instead, they stayed inside the piston bowl.

Finally, comparing combustion characteristics for cases with the Standard bowl and the Flat bowl V2, the following is observed: the CA50 of the Flat bowl V2 case remained unchanged compared to the Standard bowl; the CA90 advanced by almost 6.6 deg, as reported in Table 7.

Table 7. Comparison of the $IMEP_{gross}$, gross indicated efficiency, CA50, and CA90 for the double-side-injector concept with the standard omega-shaped piston bowl and the new Flat bowl V2.

	Standard bowl	Flat bowl V2
$IMEP_{gross}$ [bar]	23.80	24.42
GIE [%]	41.0	42.0
CA50 [deg ATDC]	11.2	11.2
CA90 [deg ATDC]	52.2	45.6

Earlier CA90 means that the HR tail is reduced with the Flat bowl V2. This, along with a slight reduction in heat transfer losses and a 0.6 %p reduction in combustion losses led to a 1 %p increase in indicated efficiency (Figure 18). Hence, the Flat bowl V2 is proven to be more effective that the Standard bowl and Flat bowl V1 and should further be improved by reducing the level of interaction between the flame plumes, thus improving the in-cylinder air utilization.

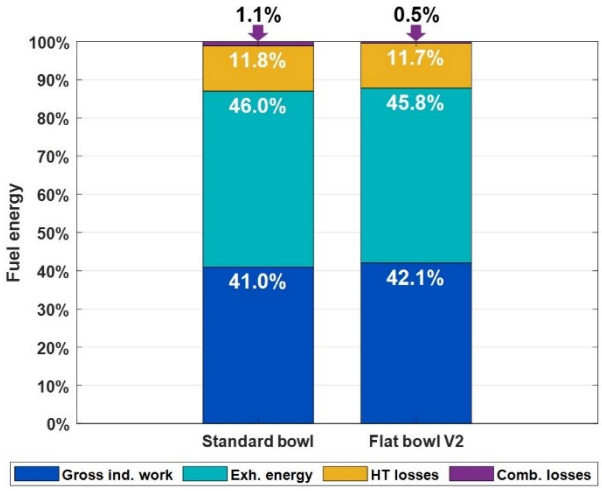

Figure 18. Fuel energy distribution between work on the piston, exhaust enthalpy, heat transfer losses, and combustion losses for the double-side-injector configuration with the standard omega-shaped piston bowl and the new Flat bowl V2.

Pancake Piston

It was previously shown in this paper that the plumes start interacting after two of them hit the wall and get directed towards the neighboring plumes. A pancake piston geometry (Figure 19) is studied as it offers a larger distance between the injector nozzle and the walls, thus has a potential to reduce plume-to-plume interactions.

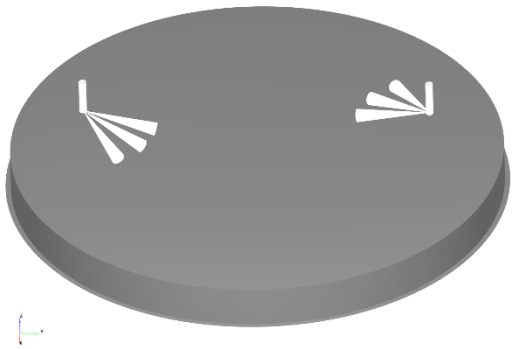

Figure 19. The double-side-injector configuration with a pancake piston geometry.

As can be seen from Figure 20, the pancake geometry did not meet the expectations. The heat release is severely limited starting from 4 deg ATDC. This is due to the fact that the flame plumes attach to the piston surface leading to their slowdown, extensive heat loss, and flame quenching. This can also be observed in Figure 21.

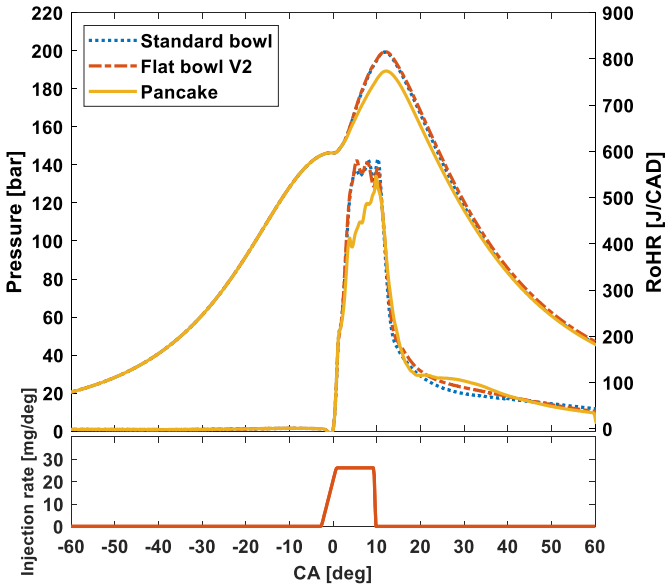

Figure 20. Injection rate, rate of heat release (RoHR), and pressure traces for the double-side-injector configuration with the standard piston bowl, Flat bowl V2, and a pancake piston.

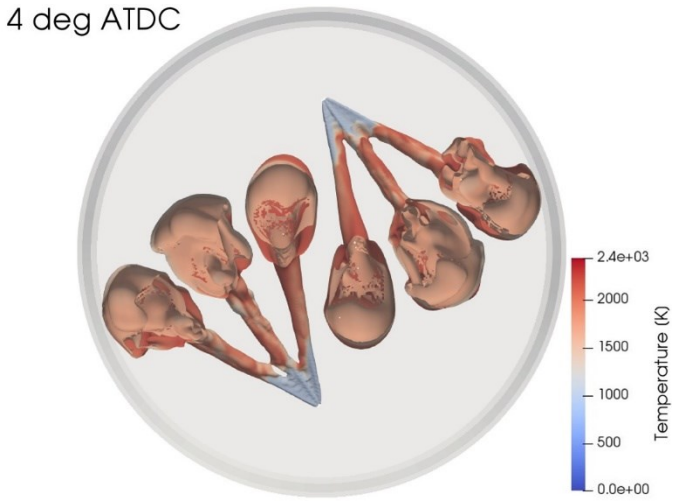

Figure 21. Flame plumes from the side injectors interacting with a pancake piston.

From Figure 22 it can also be seen that the heat losses are drastically higher with the pancake piston geometry compared to both the Flat bowl V2 and even the Standard bowl designs. The increase is mainly due to the heat flux to the cylinder liner, which is insignificant for the other cases.

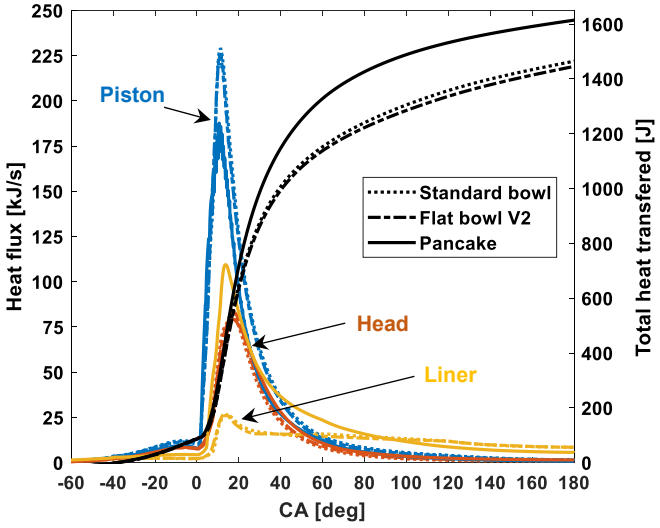

Figure 22. Heat flux to the piston, head, and liner surfaces, and the total amount of heat transferred to all cylinder walls combined for the standard omega-shaped piston bowl, Flat bowl V2, and a pancake piston geometry.

Owing to the fact that the flat shape of the piston allows the flame plumes to be pushed toward the cylinder liner, the hot temperature zones eventually end up near the liner. This results in extensive heat transfer to the liner and overall poor performance of this configuration. This suggests that the pancake piston geometry is not suitable for the fuel injection system with two side injectors.

Asymmetrical Piston Bowl V1

Inspired by the potential of the Flat bowl V2 piston geometry, we created a new asymmetrical piston bowl design, illustrated in Figure 23.

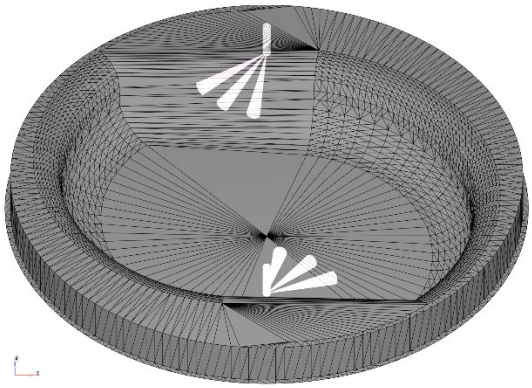

Figure 23. Asymmetrical piston bowl V1 proposed for the double-side-injector concept.

This piston shape is designed to maximize the distance between the injector and the piston surface for all six sprays but avoiding the drawbacks of the pancake piston. By increasing the distance between the nozzle # 1 (Figure 7) and the piston bowl, the extent to which two of the plumes are redirected and subsequently interact with the other plumes is minimized. As can be seen from Figure 24, Asymm. bowl V1 seems to slightly improve the RoHR shape. The tail shortens and the CA90 advanced by 5 deg (Table 8).

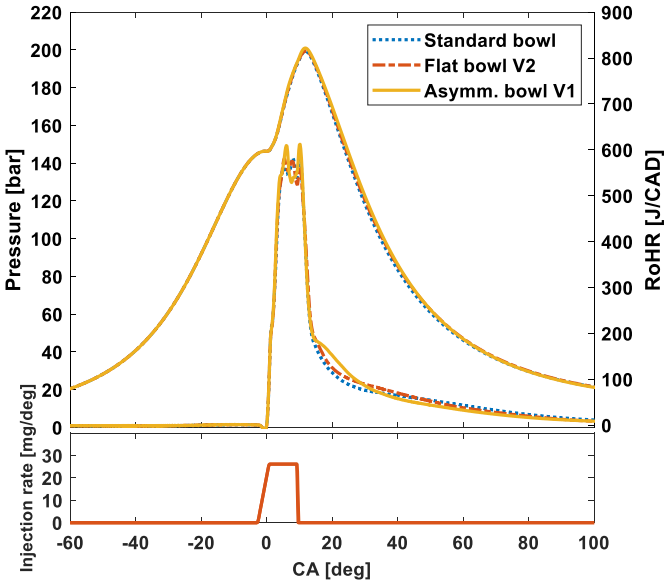

Figure 24. Injection rate, rate of heat release (RoHR), and pressure traces for the double-side-injector configuration with the standard piston bowl, Flat bowl V2, and the Asymmetrical bowl V1.

Table 8. Comparison of the CA90 for the double-side-injector concept with the standard omega-shaped piston bowl, Flat bowl V2, and Asymmetrical bowl V1.

	CA90 [deg ATDC]
Standard bowl	52.2
Flat bowl V2	45.6
Asymm. bowl V2	40.8

However, looking at Figure 25, one can observe that the heat flux to the piston increased, leading to 0.5 %p higher fraction of energy lost to heat transfer.

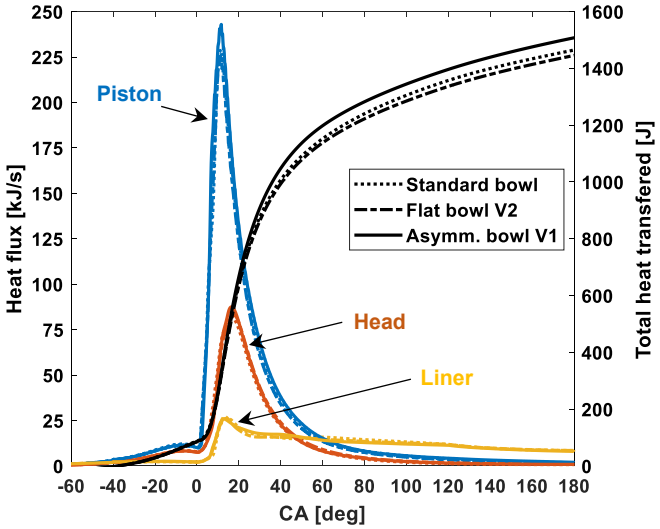

Figure 25. Heat flux to the piston, head, and liner surfaces, and the total amount of heat transferred to all cylinder walls combined for the standard omega-shaped piston bowl, Flat bowl V2, and Asymmetrical bowl V1.

Nevertheless, due to improvements in the thermodynamic cycle and hence reductions in exhaust losses, the resultant indicated efficiency increased with the Asymmetrical bowl V1 compared to the Flat bowl V2 and the Standard bowl (Figure 26).

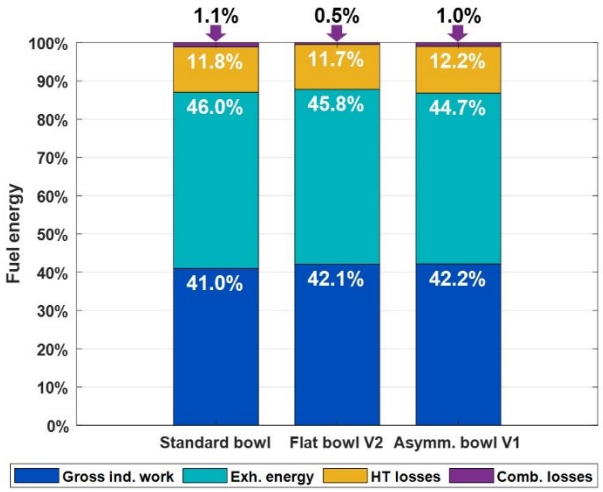

Figure 26. Fuel energy distribution between work on the piston, exhaust enthalpy, heat transfer losses, and combustion losses for the double-side-injector configuration with the standard omega-shaped piston bowl, Flat bowl V2, and Asymmetrical bowl V1.

Asymmetrical Piston Bowl V2 (Overhead Nozzle Holes)

In an attempt to further minimize the distance between the injector nozzles and any cylinder boundaries that they might face, another asymmetrical bowl shape was created (Figure 27).

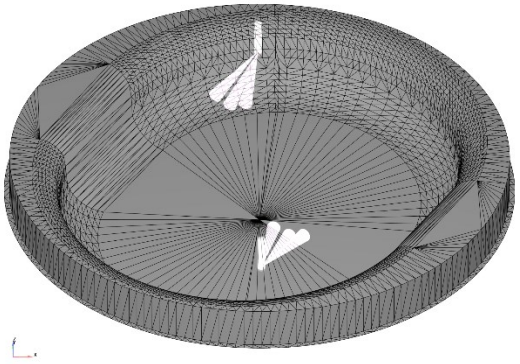

Figure 27. Asymmetrical piston bowl V2 proposed for the double-side-injector concept.

The chance of contact between the spray plumes and the piston bowl is minimized with the Asymm. bowl V2. However, the issue with the unfavorable heat release further aggravated, as can be seen in Figure 28. In the Asymm bowl V2 case, the nozzle holes are placed closer to one another in order reduce interactions between the sprays and the walls. This, on the other hand, resulted in more interactions between the sprays themselves, given the shorter distance between them, which caused higher local equivalence ratios and poor fresh air utilization (Figure 29).

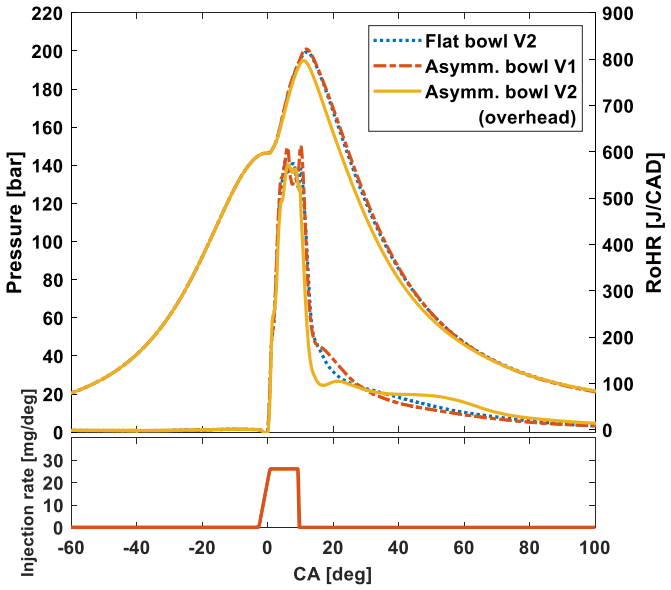

Figure 28. Injection rate, rate of heat release (RoHR), and pressure traces for the double-side-injector configuration with Flat bowl V2, Asymmetrical bowl V1, and Asymmetrical bowl V2 with overhead nozzle holes.

As can be seen in Figure 29, each set of the three spray plumes forms one relatively large reaction zone. This zone is more attached to the cylinder liner, and even extends into the crevice region. The mixing characteristics of this configuration is relatively poor, as the resultant high-temperature zones cover less volume of the combustion chamber compared to the standard central-injector configuration and even the double-side-injector configuration with the flat and asymmetrical piston bowl designs.

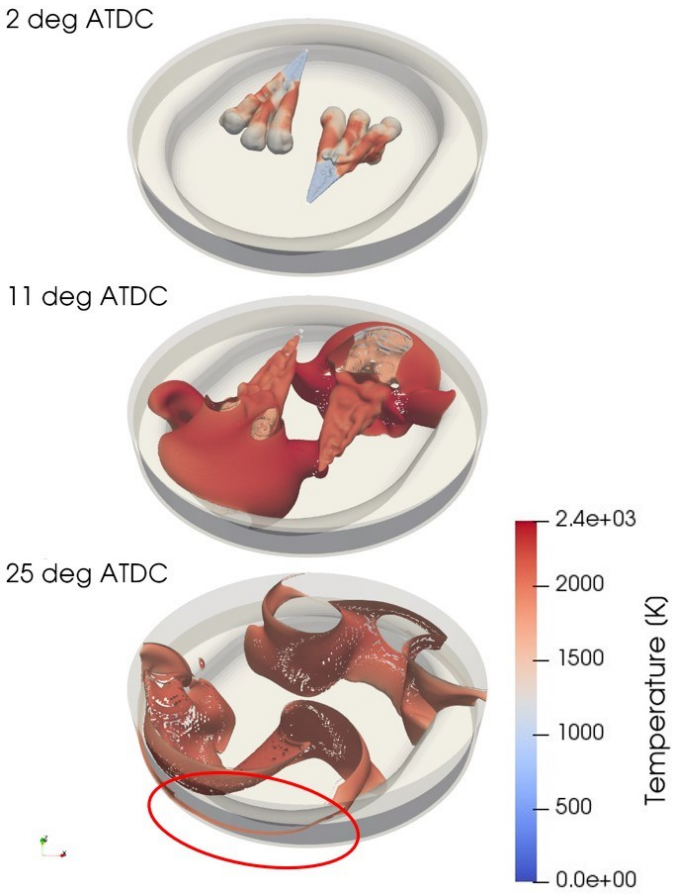

Figure 29. Flame plumes generated by the side injectors with overhead nozzle holes combined with the Asymmetrical bowl V2 piston design.

In terms of heat losses, the Asymm. Bowl V2 has a significant advantage in the beginning of the cycle owing to the reduced interaction of the plumes with the walls. However, later on this advantage is lost due to the increased losses to the cylinder liner. Eventually, the energy lost to heat transfer for the Asymm. bowl V2 in magnitude is between the Flat bowl V2 and the Asymm. bowl V2, Flat bowl V2 having the lowest values (Figure 30).

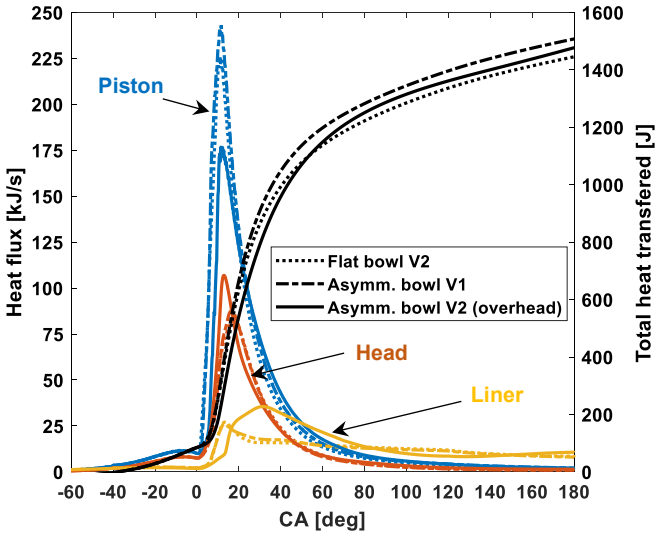

Figure 30. Heat flux to the piston, head, and liner surfaces, and the total amount of heat transferred to all cylinder walls combined for Flat bowl V2, Asymmetrical bowl V1, and Asymmetrical bowl V2 with overhead nozzle holes.

NOx Emissions

In this section, the double-side-injector concept is assessed in terms of NOx emissions. In Figure 31, the reference central injector case with a standard omega-shaped piston bowl is compared to the side injectors with the standard piston bowl and Flat bowl V1. The mean in-cylinder temperature, rate of heat release, and accumulated NOx are plotted as a function of crank angle. Note that the mean temperature showed a better correlation with the NOx emissions than the combustion temperature. This is because the combustion temperature was approximately equal for all cases, whereas the size of the high-temperature zones varied substantially.

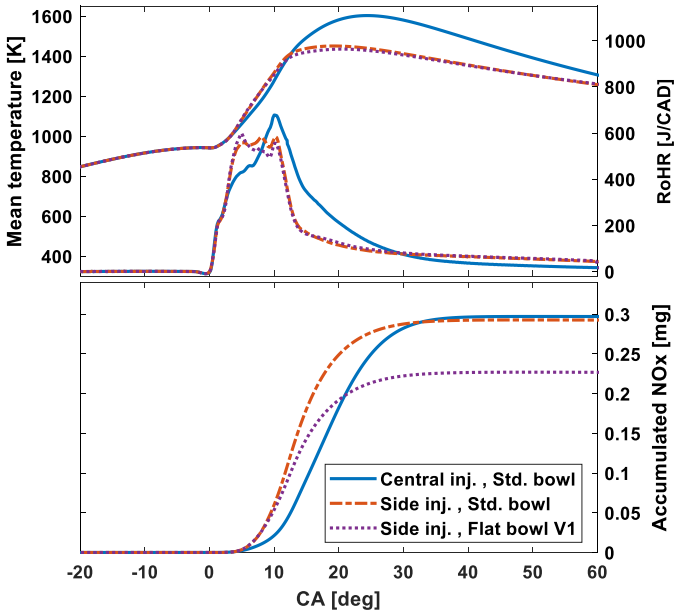

Figure 31. Mean in-cylinder temperature, rate of heat release, and accumulated NOx for the reference central injector case, the double-side-injector case with a standard piston bowl, and the double-side-injector case with Flat bowl V1.

As can been seen in Figure 31, the reference case with a single central injector showed overall the highest emissions of NOx. The double-side-injector configuration with the standard bowl showed much faster NOx production in the beginning of the cycle due to the faster heat release. However, starting from 5 cad ATDC, the heat release reached a plateau owing to the reduced mixing rates and overall smaller high-temperature zone, which, in turn, resulted in reduced NOx production and overall slightly lower NOx emissions from that cycle. Finally, the double-side-injector configuration with the Flat bowl V1 piston showed the lowest NOx emissions (25% lower than the other two cases). In the beginning of the injection process, the NOx production rate is similar for the side injectors with the standard piston bowl and the Flat bowl V1. However, once the flame plumes reach the cylinder head after bouncing off the piston bowl (Figure 15), the Flat bowl V1 case shows much lower NOx production rates. This is a consequence of the fact that for this case, the flame plumes are attached to the piston and the head, effectively reducing the area of the high-temperature stoichiometric zones which produce most of the NOx. The reason NOx kept being produced after the flame plumes had hit the piston in the conventional central injector case is the optimized shape of the piston bowl for inducing global mixing. In contrast, the axisymmetric piston bowl shape is poorly optimized for the side injectors, hence, the global mixing is substantially weaker, which leads to significantly smaller area of the stoichiometric zone. The resultant gross specific NOx emissions are presented in g/kWh in Table 9.

Table 9. Comparison of the gross specific NOx emissions from the reference central-injector case, the double-side-injector case with the standard bowl and the Flat bowl V1.

	NOx emissions [g/kWh]
Central injector, standard piston bowl	0.288
Side injectors, standard piston bowl	0.282
Side injector, Flat bowl V1	0.220

Potential Strategies for Efficiency Improvement

In this study, the main issues inherent in high-load high-EGR operation of an engine with two side injectors were identified. These issues are poor mixing characteristics, slow heat release, and, consequently, increased exhaust losses and reduced thermodynamic efficiency. These were observed to occur only at high-load and high-EGR conditions. This problem exists partly owing to a non-optimal shape of the standard piston bowl. A number of alternative piston bowl designs were proposed and tested in this study. Certain improvements were achieved, but the main underlying reasons for the slow heat release turned out to be fundamentally inherent to the side-injector concept and the idea of increasing the spray travel distance. Thus, below we propose a number of potential solutions to this issue.

Multiple Injection Events / Isobaric Combustion

The drawbacks caused by the slow heat release with side injectors have never been observed at low- to medium-load conditions. Thus, the amount of fuel injected at high loads in a single injection event ends up being concentrated in two relatively small reaction zones. This leads to higher local equivalence ratios and, consequently, slower combustion. One of the potential solutions is to split the single injection into multiple shorter injections. These need to be timed in such a way to allow the burned gas to move out of the way of the subsequent injections before they are commenced. This opens an opportunity for implementing the isobaric combustion cycle. Isobaric combustion has been proven to offer comparable or even better indicated efficiency than the CDC at a wide range of engine load conditions, including high-load operation, despite having inherently (and purposefully) long heat release and late combustion phasing [13]. It also has the advantage of lower NOx emissions and significantly reduced heat transfer losses, much like the double-side-injector concept. Combining these two technologies seems logical to both alleviate the shortcomings of the double-side-injector concept and, potentially, further enhance the advantages of both of these concepts.

Keeping the Central Injector

The issues with slow heat release with the side-injector configuration were only observed at high-load conditions. FuelMEPs below 30 bar have never been observed to cause significant mixing problems. Hence, another promising strategy is, first, to inject the amount of fuel equivalent to about 30 bar FuelMEP from the side injectors, and then inject the rest conventionally, from the central injector. The umbrella angle of the central injector will likely need to be larger than that of the side injectors in order to minimize interactions of the centrally-injected fuel with the already burning charge. This strategy may also be combined with the multiple-injection / isobaric combustion strategies for additional improvements in efficiency and emissions.

Highly Swirling In-Cylinder Flow

Swirl has long been known to promote mixing of fuel with fresh air in combustion chamber of ICEs [26-29]. In the side-injector concept swirl is expected to have even larger effect. Since injectors are placed at the rim of the piston bowl, they on their own are able to generate a significant swirling in-cylinder flow. This is demonstrated by plotting the magnitude of the velocity field along either x or y axis. Figure 32 shows velocity magnitude in y direction for the double-side-injector case with Flat bowl V1, where one can observe significantly stratified signs of the velocity field, suggesting a bulk swirling motion generated by the two injectors.

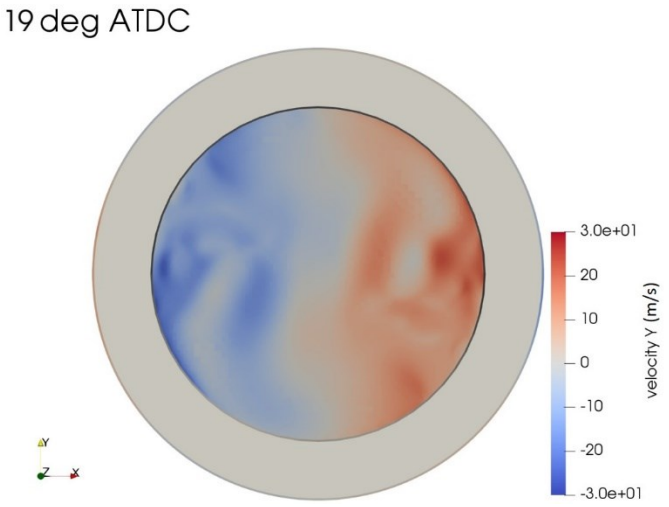

Figure 32. Velocity magnitude in y direction for the double-side-injector configuration, which demonstrates the concept's ability to generate significant swirl.

Thus, setting up a port-induced swirl prior to the start of injection in the opposite direction of the sprays is expected to generate a lot of turbulence, thus promoting mixing and accelerating burning rate.

Summary and Conclusions

In this study, three-dimensional RANS CFD model was validated against experimental data for a high-load high-EGR operating point of the combustor unit of the DCEE. Then, a number of simulations were performed in order to study the fuel injection system with two injectors placed at the rim of the piston bowl at conditions relevant to high-load engine operation. The goal of the study was to identify the challenges associated with such operation, find solutions, and establish background for later, more specific investigations. The following are the conclusions of this work:

1. A fuel injection system with two side injectors is capable of achieving high-load high-EGR operating points with satisfactory thermal efficiency.
2. Heat transfer losses are reduced by over 8% with side injectors, suggesting a better suitability of this configuration for the split-cycle DCEE concept.
3. Surface area of the piston does not significantly affect heat transfer losses at high-load operating points. Instead, the flow pattern generated by the piston bowl shape plays a major role in determining the magnitude and the spatial location of the heat losses.
4. Compared to the conventional single central injector configuration, the concept with two side injectors has 2 %p lower indicated efficiency. The main reason for this reduction is the slower heat release due to inadequate mixing characteristics at high-load high-EGR operating points.
5. Optimization of the piston bowl shape minimizes interactions between spray plumes, thus improving in-cylinder fresh air

utilization. Pancake piston is not suitable for this concept, instead, asymmetrical (non-axisymmetric) bowl geometries should be taken advantage of.

6. The double-side-injector concept combined with a flat-bowl piston design achieved a 24% reduction in NOx emissions compared to the conventional central-injector configuration.
7. The following three strategies need to be investigated in order to maximize indicated efficiency of the multiple-fuel-injector concept:
    a. Multiple injection events with isobaric combustion
    b. Distributing the injected fuel between the two side injectors and a third central injector with a different spray umbrella angle.
    c. Strong port-induced swirl in the opposite direction to the sprays from side injectors.

References

1. https://www.eea.europa.eu/data-and-maps/indicators/transport-emissions-of-greenhouse-gases/transport-emissions-of-greenhouse-gases-12
2. Babayev, Rafig, and Bengt Johansson. Should We Walk or Take a Car for Minimum Greenhouse Gas Emissions?. No. 2019-01-0996. SAE Technical Paper, 2019.
3. European Commission, “Strategy for Reducing Heavy-Duty Vehicles’ Fuel Consumption and CO2 Emissions, 2014, http://ec.europa.eu/clima/policies/transport/vehicles/heavy/docs/com_285_2014_en.pdf.
4. ExxonMobil, “The Outlook for Energy: A View to 2040,” 2016.
5. Regulation (EU) 2019/1242 of the European Parliament and of the Council of 20 June 2019 setting CO2 emission performance standards for new heavy-duty vehicles and amending Regulations (EC) No 595/2009 and (EU) 2018/956 of the European Parliament and of the Council and Council Directive 96/53/EC, http://data.europa.eu/eli/reg/2019/1242/oj
6. Cummins, C.L., Diesel's Engine: From conception to 1918. 1993: Carnot Press.
7. Clarke, J. and O'Malley, E., “Analytical Comparison of a Turbocharged Conventional Diesel and a Naturally Aspirated Compact Compression Ignition Engine both Sized for a Highway Truck,” SAE Technical Paper 2013-01-1736, 2013, doi:10.4271/2013-01-1736.
8. Phillips, F., Gilbert, I., Pirault, J.-P., and Megel, M., Scuderi Split Cycle Research Engine: Overview, Architecture and Operation. SAE Int. J. Engines, 2011. 4(1)
9. Branyon, D. and Simpson, D., “Miller Cycle Application to the Scuderi Split Cycle Engine (by Downsizing the Compressor Cylinder),” SAE Technical Paper 2012-01-0419, 2012, doi:10.4271/2012-01-0419.
10. Ricardo advancing with two novel heavy-duty vehicle technologies: cryogenic split-cycle engine and microwave fuel reforming. 2013 [cited 2013; Available from: http://www.greencarcongress. com/2013/09/20130904-ricardo.html.
11. Lam, Nhut, et al. “Double Compression Expansion Engine Concepts: A Path to High Efficiency.” SAE International Journal of Engines, vol. 8, no. 4, 2015, pp. 1562–1578. JSTOR, www.jstor.org/stable/26278054
12. Lam, N., Tunestal, P., and Andersson, A., “Simulation of System Brake Efficiency in a Double Compression-ExpansionEngine-Concept (DCEE) Based on Experimental Combustion Data,” SAE Technical Paper 2019-01-0073, 2019, doi:10.4271/2019-01-0073.
13. Babayev, R., Ben Houidi, M., Andersson, A., and Johansson, B., “Isobaric Combustion: A Potential Path to High Efficiency, in Combination with the Double Compression Expansion Engine (DCEE) Concept,” SAE Technical Paper 2019-01-0085, 2019, doi:10.4271/2019-01-0085.
14. Babayev, R., Houidi, M., Shankar, V., Aljohani, B. et al., "Injection Strategies for Isobaric Combustion," SAE Technical Paper 2019-01-2267, 2019.
15. Merkel, S., Eckert, P., Wagner, U., Velji, A. et al., "Investigation of a New Injection Strategy for Simultaneous Soot and NOx Reduction in a Diesel Engine with Direct Injection," SAE Int. J. Fuels Lubr. 1(1):1433-1442, 2009, https://doi.org/10.4271/2008-01-1790.
16. Wagner, Uwe, and Ulrich Spicher. "Advanced heterogeneous diesel combustion with ultra-low engine emissions and low fuel consumption levels." Proceedings of the Institution of Mechanical Engineers, Part D: Journal of Automobile Engineering 227, no. 1 (2013): 110-119.
17. Okamoto, Takeshi, and Noboru Uchida. "New concept for overcoming the trade-off between thermal efficiency, each loss and exhaust emissions in a heavy duty diesel engine." SAE International Journal of Engines 9, no. 2 (2016): 859-867.
18. Nyrenstedt, Gustav, Tariq Lutfallah Mohammed Alturkestani, Hong G. Im, and Bengt Johansson. "CFD Study of Heat Transfer Reduction Using Multiple Injectors in a DCEE Concept." (2019).
19. Richards, K. J., Senecal, P. K., and Pomraning, E., CONVERGE (v2.4), Convergent Science, Inc., Madison, WI (2017).
20. Sarathy, M., Atef, N., Alfazazi, A., Badra, J. et al., "Reduced Gasoline Surrogate (Toluene/n-Heptane/iso-Octane) Chemical Kinetic Model for Compression Ignition Simulations," SAE Technical Paper 2018-01-0191, 2018, https://doi.org/10.4271/2018-01-0191.
21. Amsden, A.A., "KIVA-3V: A Block Structured KIVA Program for Engines with Vertical or Canted Valves," Los Alamos National Laboratory Technical Report LA-13313-MS, 1997.
22. Heywood, J.B., Internal Combustion Engine Fundamentals, McGraw Hill, Inc., 1988
23. Law, Chung K. Combustion physics. Cambridge university press, 2010.
24. A. Henderson, ParaView Guide, A Parallel Visualization Application. Kitware Inc., 2007
25. Nyrenstedt, G., Im, H., Andersson, A., and Johansson, B., “Novel Geometry Reaching High Efficiency for Multiple Injector Concepts,” SAE Technical Paper 2019-01-0246, 2019, doi:10.4271/2019-01-0246.
26. Espey, C., J. A. Pinson, and T. A. Litzinger. "Swirl effects on mixing and flame evolution in a research DI diesel engine." SAE transactions (1990): 2079-2088.
27. McCracken, Michael E., and J. Abraham. "Swirl-spray interactions in a diesel engine." SAE Transactions (2001): 882-898.
28. Li, Xiangrong, Zuoyu Sun, Wei Du, and Rong Wei. "Research and development of double swirl combustion system for a DI diesel engine." Combustion Science and Technology 182, no. 8 (2010): 1029-1049.
29. Johansson, Bengt. Combustion Engines. Department of Energy Sciences, Lund University, 2014.

Contact Information

Rafig Babayev
Clean Combustion Research Center (CCRC)
King Abdullah University of Science and Technology (KAUST)
Building 5, 4204-WS10, Thuwal 23955-6900,
Saudi Arabia
rafig.babayev@kaust.edu.sa
rafik.babayev95@gmail.com
+966560249272

Definitions/Abbreviations

%p: percent points

AMR: adaptive mesh refinement

ATDC: after top dead center

CA: crank angle

CA50: crank angle at which 50% of the total heat of combustion has been released

CA90: crank angle at which 90% of the total heat of combustion has been released

CAD: crank angle degree

CDC: conventional diesel combustion

CFD: computational fluid dynamics

CI: compression ignition

CO2: carbon dioxide

DCEE: double compression-expansion engine

EGR: exhaust gas recirculation

FuelMEP: fuel mean effective pressure

GIE: gross indicated efficiency

HD: heavy-duty

HP: high-pressure

HR: heat release

HT: heat transfer

$IMEP_{gross}$: gross indicated mean effective pressure

LP: low-pressure

NOx: oxides of nitrogen

RANS: Reynolds-averaged Navier-Stokes

RoHR: rate of heat release

RPM: revolutions per minute

Acknowledgments

This work was sponsored by King Abdullah University of Science and Technology (KAUST) and supported by the KAUST Supercomputing Laboratory (KSL). All simulations were performed on KSL's Shaheen II supercomputer using CONVERGE CFD software. Convergent Science provided CONVERGE licenses and technical support for this work.

The authors would also like to thank Dr. Nhut Lam from Lund University for providing experimental data for validation of CFD models.